In vivo vasculogenic potential of human blood-derived endothelial progenitor cells

Juan M. Melero-Martin,[1] Zia A. Khan,[1] Arnaud Picard,[1] Xiao Wu,[1] Sailaja Paruchuri,[1] and Joyce Bischoff[1]

[1]Vascular Biology Program and Department of Surgery, Children's Hospital, Boston, Harvard Medical School, Boston, MA

Vascularization of tissues is a major challenge of tissue engineering (TE). We hypothesize that blood-derived endothelial progenitor cells (EPCs) have the required proliferative and vasculogenic activity to create vascular networks in vivo. To test this, EPCs isolated from human umbilical cord blood or from adult peripheral blood, and human saphenous vein smooth muscle cells (HSVSMCs) as a source of perivascular cells, were combined in Matrigel and implanted subcutaneously into immunodeficient mice. Evaluation of implants at one week revealed an extensive network of human-specific lumenal structures containing erythrocytes, indicating formation of functional anastomoses with the host vasculature. Quantitative analyses showed the microvessel density was significantly superior to that generated by human dermal microvascular endothelial cells (HDMECs) but similar to that generated by human umbilical vein endothelial cells (HUVECs). We also found that as EPCs were expanded in culture, their morphology, growth kinetics, and proliferative responses toward angiogenic factors progressively resembled those of HDMECs, indicating a process of in vitro maturation. This maturation correlated with a decrease in the degree of vascularization in vivo, which could be compensated for by increasing the number of EPCs seeded into the implants. Our findings strongly support the use of human EPCs to form vascular networks in engineered organs and tissues. (Blood. 2007; 109:4761-4768)

Introduction

Tissue engineering (TE) holds promise as a new approach for creating replacement tissue to repair congenital defects or diseased tissue.[1] One strategy is to seed the appropriate cells on a biodegradable scaffold engineered with the desired mechanical properties, followed by stimulation of cell growth and differentiation in vitro, such that, on implantation in vivo, the engineered construct undergoes remodeling and maturation into functional tissue.[2] Examples of this approach include blood vessels and cardiovascular substitutes, where autologous vascular cells have been used for this purpose without immune rejection.[3-5] Despite advances in this field, TE still faces important constraints. There are no TE constructs presently available that have an inherent microvascular bed ready to be connected to the host vascular system. Consequently, tissues implanted with a volume more than 2 to 3 mm^3 cannot obtain appropriate provision of nutrients, gas exchange, and elimination of waste products since all these mechanisms are limited by the diffusion distance.[6] To overcome the problem of vascularization, strategies such as embedding angiogenic factors into the scaffold to promote ingrowth of microvessels, fabrication technologies to create polymers containing vessel-like networks, and prevascularization of matrices prior to cell seeding have been proposed.[7-11]

The need for prefabricated channels or growth factor–induced angiogenesis could be avoided by exploiting the inherent vasculogenic ability of endothelial cells (ECs). Using human umbilical vein ECs (HUVECs), microvascular networks in collagen/fibronectin gels were formed within 31 days of implantation into immunodeficient mice.[12] Similar results have been reported with human microvascular ECs (HDMECs) seeded on biopolymer matrices, where functional microvessels were evident 7 to 10 days after implantation into mice.[13] Nevertheless, the clinical use of mature ECs derived from autologous vascular tissue presents some important limitations: (1) the isolation relies on an invasive procedure, (2) mature ECs show relatively low proliferative potential, and (3) it is difficult to obtain a sufficient number of cells from a small biopsy of autologous tissue. These limitations have instigated the search for other sources of ECs with more proliferative and vasculogenic activities such as those derived from both embryonic and adult stem and progenitor cells.[14] One recent example showed how seeding of endothelial cells derived from embryonic stem cells along with myoblast and embryonic fibroblasts resulted in the formation of skeletal muscle tissue.[15] However, ethical considerations along with a poor understanding of the mechanisms controlling the differentiation of embryonic stem cells are hurdles that need to be overcome before these cells can be used in a clinical setting.

For clinical applications, the presence of endothelial progenitor cells (EPCs) in circulation represents a promising opportunity to noninvasively obtain the required endothelial population.[16] In previous work, we showed the creation of microvascular networks in vitro using biodegradable scaffolds seeded with EPCs that had been isolated from human umbilical cord blood and expanded in vitro as mature ECs.[17] Using a sheep model, we also showed that blood-derived EPCs could endothelialize small-diameter blood vessels.[5] We now propose that human blood-derived EPCs constitute a robust source of ECs with the potential to form functional

Submitted December 15, 2006; accepted February 5, 2007. Prepublished online as *Blood* First Edition Paper, February 27, 2007; DOI 10.1182/blood-2006-12-062471.

The online version of this article contains a data supplement.

The publication costs of this article were defrayed in part by page charge payment. Therefore, and solely to indicate this fact, this article is hereby marked "advertisement" in accordance with 18 USC section 1734.

capillary networks in vivo. To test this, we used a xenograft model where human cells were mixed in Matrigel and implanted subcutaneously into immunodeficient mice. Our goal was to advance feasibility studies by evaluating the ease with which highly purified and phenotypically defined human EPCs can create microvascular structures that form functional anastomoses with the host vasculature.

Material and methods

Isolation and culture of blood-derived EPCs

Human umbilical cord blood was obtained from the Brigham and Women's Hospital in accordance with an institutional review board–approved protocol. Adult peripheral blood was collected from volunteer donors in accordance with a protocol approved by Children's Hospital Boston Committee on Clinical Investigation and was obtained with informed consent according to the Declaration of Helsinki and under a protocol approved by the Committee on Clinical Investigation. Both cord blood–derived EPCs (cbEPCs) and adult peripheral blood–derived EPCs were obtained from the mononuclear cell (MNC) fractions, in a similar manner as used in previous studies.[18-20] MNCs were seeded on 1% gelatin-coated tissue culture plates using endothelial basal medium (EBM-2) supplemented with SingleQuots (except for hydrocortisone) (Cambrex Bio-Science, Walkersville, MD), 20% FBS (Hyclone, Logan, UT), 1 × glutamine-penicillin-streptomycin (GPS; Invitrogen, Carlsbad, CA), and 15% autologous plasma.[17] Unbound cells were removed at 48 hours for cord blood and at 4 days for adult blood. In both cases, the bound cell fraction was then maintained in culture using EBM-2 supplemented with 20% FBS, SingleQuots (except for hydrocortisone), and 1 × GPS (this medium is referred to as EBM-2/20%). Colonies of endothelial-like cells were allowed to grow until confluence, trypsinized, and purified using CD31-coated magnetic beads (Dynal Biotech, Brown Deer, WI) (Figures S1 and S5, available on the *Blood* website; see the Supplemental Materials link at the top of the online article). CD31-selected EPCs were serially passaged and cultured on fibronectin (FN)–coated (1 μg/cm^2; Chemicon International, Temecula, CA) plates at 5×10^3 cell/cm^2 in EBM-2/20%. HDMECs from newborn foreskin cultured in the same condition as cbEPCs were used as positive controls.[21] Human saphenous vein smooth muscle cells (HSVSMCs) grown in DMEM (Invitrogen), 10% FBS, 1 × GPS, and 1 × nonessential amino acids (Sigma-Aldrich, St Louis, MO) were used as negative controls for endothelial phenotype.

Phenotypic characterization of cbEPCs

Methods for flow cytometry, indirect immunofluorescence, and reverse-transcription–polymerase chain reaction (RT-PCR) are described in Document S1.

In vitro maturation of cbEPCs

Expansion potential of cbEPCs. cbEPCs and adult EPCs, isolated as described in "Isolation and culture of blood-derived EPCs," were expanded for 112 and 60 days, respectively. All passages were performed by plating the cells onto 1 μg/cm^2 FN-coated tissue culture plates at 5×10^3 cell/cm^2 using EBM-2/20%. Medium was refreshed every 2 to 3 days and cells were harvested by trypsinization and replated in the same culture conditions for the next passage. Cumulative values of total cell number were calculated by counting the cells at the end of each passage using a hemocytometer.

Growth kinetics assay. Growth curves of cbEPCs were evaluated at different passages. Cells were plated in triplicates onto 1 μg/cm^2 FN-coated 24-well tissue culture plates at 5×10^3 cell/cm^2 in 0.5 mL EBM-2/20%. Medium was refreshed every 2 days and cell numbers were evaluated at 24-hour intervals for 7 days by counting the cells after trypsinization using a hemocytometer. Doubling time profiles were calculated from the mean values obtained from each growth curve at different passages.[22]

Cell size measurements. Morphologic differences of cbEPCs were evaluated at different passages. Confluent cell monolayers were immunostained with VE-cadherin antibody for cell surface and DAPI for nuclear visualization as described in Document S1. The areas occupied by cell bodies and cell nuclei were measured by analysis (ImageJ software; NIH, Bethesda, MD) of the images obtained from randomly selected fields from 3 separate cultures after immunostaining. All values were normalized to the value of total cell area.

Proliferation assay. Cells were seeded in triplicates onto 1 μg/cm^2 FN-coated 24-well plates at 5×10^3 cell/cm^2 using EMB-2 supplemented with 5% FBS and 1 × GPS (control medium); plating efficiency was determined at 24 hours, then cells were treated for 48 hours using control medium in the presence or absence of either 10 ng/mL VEGF-A (R&D Systems, Minneapolis, MN) or 1 ng/mL bFGF (Roche Applied Science, Indianapolis, IN). Cells were trypsinized and counted using a hemocytometer. Values were normalized to the cell numbers determined at 24 hours.

In vivo vasculogenesis experiments

Matrigel implantations. Unless otherwise indicated, 1.5×10^6 EPCs were mixed with 0.375×10^6 HSVSMCs (4:1 ratio) and resuspended in 200 μL phenol red–free Matrigel (BD Bioscience, San Jose, CA) on ice. The mixture was implanted on the back of a 6-week-old male athymic nu/nu mouse (Charles River Laboratories, Boston, MA) by subcutaneous injection using a 25-gauge needle. One implant was injected per mouse. Each experimental condition was performed with 4 mice.

Histology and immunohistochemistry. Matrigel implants were removed at one week after xenografting, fixed in 10% buffered formalin overnight, embedded in paraffin, and sectioned. Hematoxylin and eosin (H&E)–stained 7-μm–thick sections were examined for the presence of lumenal structures containing red blood cells. For immunohistochemistry, 7-μm–thick sections were deparaffinized, blocked for 30 minutes in 5% horse serum, and incubated with human-specific CD31 monoclonal antibody (1:50; DakoCytomation, Carpinteria, CA), anti–human α-SMA (1:750; Sigma-Aldrich), or mouse IgG (DakoCytomation) for 1 hour at room temperature. Horseradish peroxidase–conjugated secondary antibody and 3,3′-diaminobenzidine (DAB) were used for detection. The sections were counterstained with hematoxylin and mounted using Permount (Fisher Scientific, Hampton, NH). Images were taken with a Nikon Eclipse TE300 (Nikon, Melville, NY) using Spot Advance 3.5.9 software (Diagnostic Instruments, Sterling Heights, MI) and a 10×/0.45 objective lens. Images were assembled into multipanel figures using Adobe Illustrator CS 11.0.0 (Adobe Systems, San Jose, CA).

Microvessel density analysis. Microvessels were detected by the evaluation of H&E-stained sections taken from the middle part of the implants. The full area of each individual section was evaluated. Microvessels were identified and counted as lumenal structures containing red blood cells. The area of each section was estimated by image analysis. Microvessel density was calculated by dividing the total number of red blood cell–filled microvessels by the area of each section (expressed as vessels/mm^2). Values reported for each experimental condition correspond to the average values obtained from 4 individual animals.

Statistical analysis

The data were expressed as means ± SD. Where appropriate, data were analyzed by analysis of variance (ANOVA) followed by 2-tailed Student unpaired *t* tests. *P* values below .05 were considered to indicate a statistically significant difference.

Results

Phenotypic characterization of cbEPCs

We isolated EPCs from the MNC fraction of human umbilical cord blood samples (n = 19) in a similar manner as used in previous studies.[18,19] Cord blood–derived endothelial colonies (identified by typical cobblestone morphology) emerged in culture after one

week (Figure S1). The size, frequency, and time of appearance of these colonies varied as already reported[18] (data not shown). Endothelial colonies were left to grow in the original culture plates until confluence and purified thereafter (at passage 1) by selection of $CD31^+$ cells (Figure S1). This procedure resulted in superior cell yields compared with our previous isolation protocol based on double selection of $CD34^+/CD133^+$ cells from the MNC fraction.[17] However, since CD31 is not a specific marker of EPCs and due to the heterogeneity of blood preparations, both phenotypical and functional characterization were performed. This was especially important considering that earlier studies have shown that some EPC colonies isolated from MNCs contain cells that express the hematopoietic-specific cell-surface antigen CD45,[14,23,24] raising questions about the cellular origin of circulating EPCs.

The endothelial phenotype of the isolated cbEPCs was confirmed by different methods. Flow cytometric analysis of cbEPCs showed remarkably uniform expression of EC markers CD34, VEGF-R2, CD146, CD31, VWF, and CD105 (Figure 1A). In addition, cells were negative for mesenchymal marker CD90 and hematopoietic markers CD45 and CD14, confirming that the cells were not contaminated with either mesenchymal or hematopoietic cells. Additionally, RT-PCR analyses showed the expression of EC markers CD34, VEGF-R2, CD31, VE-cadherin, VWF, and eNOS at the mRNA level (Figure 1B). Indirect immunofluorescent staining was performed to further examine the expression of EC markers. The results showed that cbEPCs expressed CD31, VE-cadherin, and VWF (Figure 1C). Of importance, the localization of CD31 and VE-cadherin at the cell-cell borders and VWF in a punctuate pattern in the cytoplasm showed clear indications of EC properties.

In addition, we tested whether cbEPCs were able to up-regulate leukocyte adhesion molecules in response to the inflammatory cytokine TNF-α. The low-to-undetectable levels of E-selectin, ICAM-1, and VCAM-1 in the untreated cbEPC cultures were up-regulated upon 5 hours of incubation with TNF-α (Figure 1D). This response to an inflammatory cytokine is characteristic of ECs and suggests that the use of cbEPC in the formation of microvascular vessels could also provide physiologic proinflammatory properties.

In summary, this combination of analyses provides a definitive demonstration that the cells isolated from umbilical cord blood were ECs and discards the possibility of hematopoietic/monocytic cells in the culture.[20] Based on the isolation methodology and the phenotypical characteristics, our isolated cells are similar to those referred to by other authors as late EPCs or endothelial outgrowth cells.[19,24] The characterization depicted in Figure 1 corresponded to cbEPCs at passage 6. However, a detailed characterization was performed at passages 4, 9, 12, and 15 with similar results (Figure

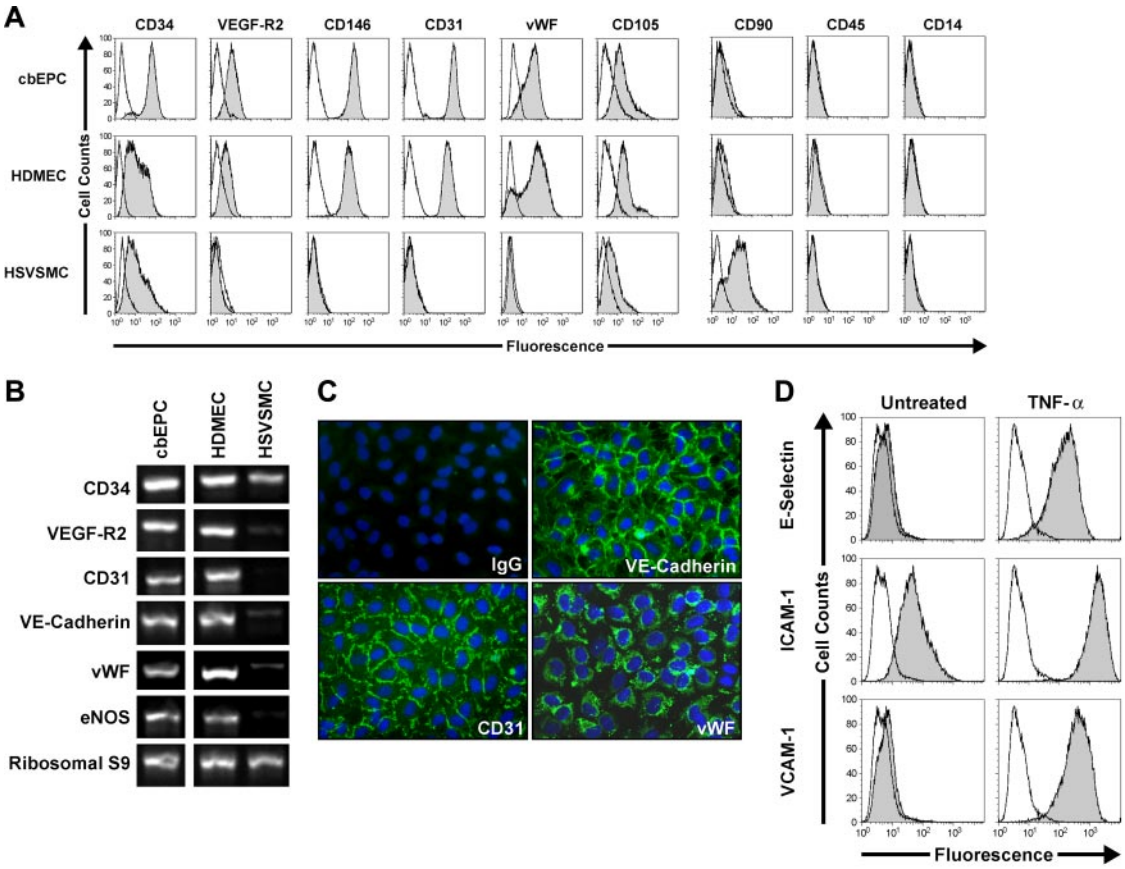

Figure 1. Phenotypic characterization of EPCs. CD31-selected cbEPCs were evaluated at passage 6. HDMECs and HSVSMCs served as positive and negative controls, respectively. (A) Cytometric analysis of cultured cbEPCs for endothelial markers CD34, VEGF-R2, CD146, CD31, VWF, and CD105, the mesenchymal marker CD90, and hematopoietic/monocytic markers CD45 and CD14. Solid gray histograms represent cells stained with fluorescent antibodies. Isotype-matched controls are overlaid in a black line on each histogram. (B) RT-PCR analysis of cbEPCs for endothelial markers CD34, VEGF-R2, CD31, VE-cadherin, VWF, and eNOS (the lanes were rearranged from the same picture to match panel A). (C) Indirect immunofluorescence of cultured cbEPCs grown in confluent monolayer showing positive staining for CD31, VE-cadherin, and VWF. VECTASHIELD mounting medium with 4,6 diamidino-2-phenylindole (DAPI; Vector Laboratories) was used. Images were taken with a Nikon Eclipse TE300 (Nikon, Melville, NY) using Spot Advance 3.5.9 software (Diagnostic Instruments) and a 20×/0.45 objective lens. Images were assembled into multipanel figures using Adobe Illustrator CS 11.0.0. (D) Up-regulation of E-selectin, ICAM-1, and VCAM-1 in cultured cbEPCs in response to TNF-α. Solid gray histograms represent cells stained with fluorescent antibodies, while black lines correspond to the isotype-matched control fluorescent antibodies.

S2A-D), indicating a stable endothelial phenotype through long-term culture. Furthermore, we provide additional characterization of the cbEPCs at passage 6 (Figure S3) to show that cbEPCs express 2 other VEGF receptors, neuropilin-1 and Flt-1 (panel A), and that the cbEPCs do not express the smooth muscle/mesenchymal cell markers PDGF-Rβ (panel B), α-SMA, or calponin (panel C).

In vivo vasculogenic potential of cbEPCs

Our previous work showed the creation of microvascular network in vitro by culturing cbEPCs and HSVSMCs on biodegradable scaffolds.[17] To answer the question of whether cbEPCs were capable of forming functional capillary networks in vivo, we implanted cbEPCs in Matrigel subcutaneously into nude mice for one week. For this experiment, 1.5×10^6 cbEPCs (passage 6) were combined with 0.375×10^6 HSVSMCs in 200 μL Matrigel, resulting in a ratio of cbEPCs to HSVSMCs of 4 to 1, and injected subcutaneously. This ratio of cbEPCs to HSVSMCs was less than the 1:1 ratio previously used,[17] with the intention to minimize the contribution of smooth muscle cells. After harvesting the Matrigel implants, H&E staining revealed the presence of lumenal structures containing murine erythrocytes throughout the implants (Figure 2A). Similar results were obtained with cbEPCs isolated from 3 different cord blood samples, yielding an average of 47.5 ± 8 microvessels/mm^2 (data not shown). Of importance, implants with either cbEPCs or HSVSMCs alone failed to form any detectable microvessels after one week (Figure 2B-C). Injections of Matrigel alone resulted in the appearance of few host cells infiltrated into the borders of the implants (Figure 2D), indicating that Matrigel itself was not responsible for the presence of vascular structures within the implants.

To further characterize the microvascular structures detected, sections of the implant were immunohistochemically stained using a human-specific CD31 antibody. As depicted in Figure 2K, nearly all of the lumenal structures stained positive for human CD31, confirming that those lumens were formed by the implanted human cbEPCs and not by the host cells. This result was important because it demonstrated that the formation of microvascular vessels within the implant is the result of a process of in vivo vasculogenesis carried out by the implanted cells and it is not due to blood vessel invasion and sprouting (ie, an angiogenic response from nearby host vasculature). The specificity of the anti–human CD31 antibody[25,26] was confirmed by the negative reaction obtained when mouse lung tissue sections were stained in parallel (Figure S4). Taken together, the human endothelial identity of the lumenal structures (Figure 2K) and the presence of murine erythrocytes within those structures (Figure 2A,H,J), it was evident that vasculogenesis occurred and, in addition, the newly created microvessels formed functional anastomoses with the host circulatory system. Next, the time course of vasculogenesis in the Matrigel was analyzed by harvesting implants at 2, 4, and 7 days after xenografting. At 2 days, a low degree of cellular organization was seen (Figure 2E). At 4 days, a high degree of organization with clear alignment of cells throughout the implant was observed, suggesting formation of cellular cords (Figure 2F). The presence of functional microvascular vessels, defined by the presence of red blood cells within the lumen, was appreciable one week after implantation (Figure 2G-H,J).

The location of the HSVSMCs was also examined by immunohistochemical staining using anti–α-SMA. Smooth muscle cells were detected both around the lumenal structures and throughout the Matrigel implants (Figure 2L), suggesting an ongoing process of vessel maturation and stabilization.[27-29] However, the α-SMA antibody is not human specific, as shown by the positive staining of control tissue sections obtained from mouse lung (Figure S4). Therefore, the observed α-SMA–positive cells could have corresponded to the implanted HSVSMCs or murine cells recruited from the host, or a combination of these.

Maturation of cbEPCs during in vitro expansion

cbEPCs were serially passaged to determine their expansion potential. Remarkably, 10^{14} cells could theoretically be obtained after only 40 days in culture, and thereafter cells were expanded up to 70 population doublings (Figure 3A), which is consistent with previous studies.[18] Significant expansion of adult blood EPCs (10^8 cells) was also achieved under the same conditions using 50 mL adult peripheral blood (Figure 3A). In addition to this enormous proliferative capacity, cbEPCs expressed and maintained a definitive endothelial phenotype in vitro as shown in Figure 1. However, neither the expansion potential nor the phenotypical stability rules out the possibility of cbEPCs undergoing cellular changes during their expansion in vitro. To investigate potential changes, the growth kinetics of cbEPCs at different passages were examined by the generation of growth curves (Figure 3B). We found that cells from earlier passages presented superior growth kinetics and reached higher cell densities at confluence. The former was

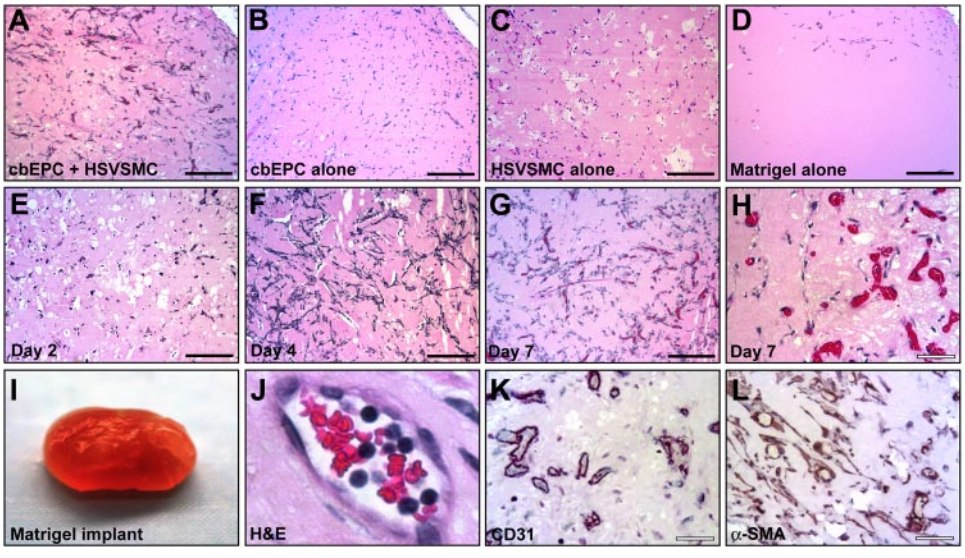

Figure 2. In vivo vasculogenic potential of EPCs. Matrigel implants containing cbEPCs and/or HSVSMCs evaluated after one week. (A) H&E staining of implants (×100) containing a combination of cbEPCs (passage 6) and HSVSMCs, (B) only cbEPCs, (C) only HSVSMCs, (D) and Matrigel alone. H&E staining of implants containing both cbEPCs and HSVSMCs evaluated at day 2 (E), day 4 (F), and day 7 (G, ×100; H, ×400) after xenografting. (I-L) Matrigel plug containing cbEPCs and HSVSMCs harvested one week after implantation. (I) Macroscopic view of explanted Matrigel plug. (J) H&E staining showing high-power view of one microvessel containing hematopoietic cells. (K) Immunohistochemical staining at one week with human-specific CD31 antibody (×400) and with (L) α-SMA antibody. All images are representative of implants harvested from 4 different animals. (Black scale bar represents 250 μm; white scale bar, 50 μm.)

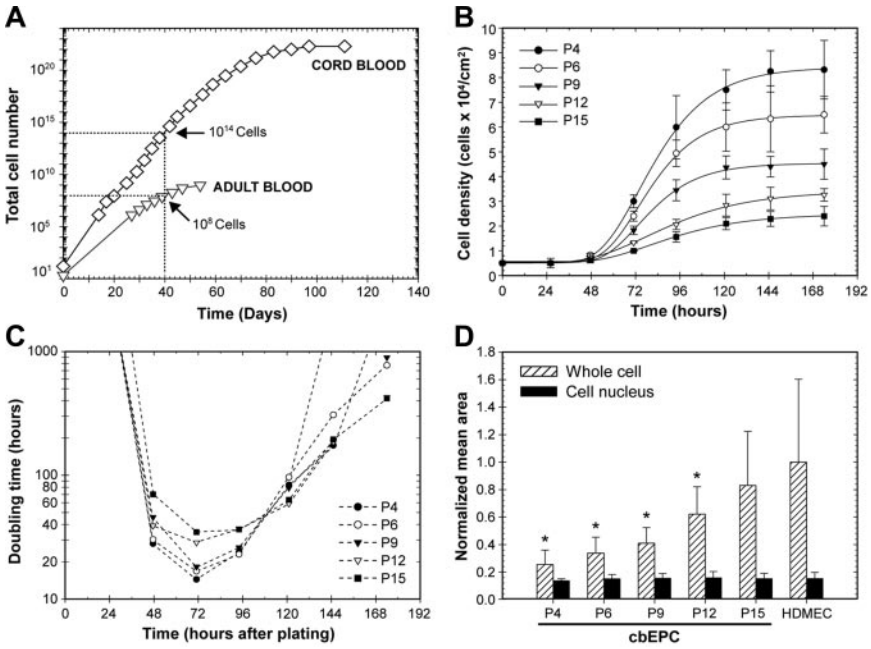

Figure 3. Growth kinetics and in vitro expansion of EPCs. (A) In vitro expansion of cbEPCs and adult blood EPCs isolated from mononuclear cells and purified by $CD31^+$ selection. (B) Growth curves of cbEPCs at different passage numbers (P4, P6, P9, P12, and P15). Each data point represents the mean of 3 separate cultures ± SD. (C) Doubling time profiles of cbEPCs at different passage numbers. Values were calculated from the mean values of cell number obtained at specific time points after plating. (D) Morphologic differences of cbEPCs at increasing passage. Each bar represents the mean area ± SD obtained from randomly selected fields. All values were normalized to the total cell area occupied by HDMECs. *$P < .05$ compared with HDMECs.

confirmed by the generation of the doubling time profiles (Figure 3C), where lower passage number corresponded with shorter doubling times. The u shape of these profiles is the result of mechanisms controlling cell growth in vitro: longer doubling times were found during both the early and late stages of the culture corresponding to the initial lag phase and the inhibition of cell growth by cell-cell contacts, respectively. Taking the minimum values as representative of the dividing capacity, cbEPCs presented minimum doubling times of 14, 17, 18, 29, and 35 hours at passages 4, 6, 9, 12, and 15, respectively. These results illustrated the remarkable dividing capacity of cbEPCs at low passage numbers, and showed that as cbEPCs were expanded in vitro, their growth kinetics progressively slowed.

Serially passaging of cbEPCs also resulted in evident morphologic differences. As they were expanded, cells progressively occupied larger areas in culture (Figure 3D). While the areas occupied by the cell nuclei remained constant at each passage, cbEPCs were found to be significantly ($P < .05$) smaller than the control HDMECs, with the exception of passage 15. As cbEPCs were expanded in vitro, the average area occupied by the cells increased toward that of HDMECs. The mean area of cbEPCs ranged from values 75% smaller than HDMECs at passage 4 to 17% smaller at passage 15. These results were consistent with the differences found in cell density at confluence (Figure 3B).

We next compared the proliferative response of cbEPCs at different passages with stimulation by angiogenic factors VEGF or bFGF (Figure 4). We found that both angiogenic factors produced a proliferative response in all the cases evaluated compared with basal proliferation in the presence of 5% serum (control). The response was statistically significant ($P < .05$) in all the groups treated with bFGF. Of interest, the proliferative response to bFGF was progressively reduced as passage number increased, and ranged from 5.4-fold at passage 4 to 2-fold at passage 15. When compared with HDMECs, the response toward bFGF was found to be significantly higher in cbEPCs at passages 4, 6, and 9, but not in the later passages. In the case of VEGF treatment, the response was statistically significant ($P < .05$) at passages 4 and 6 compared with basal proliferation. Again, the proliferative response was progressively reduced as passage number increased, and varied from 3.1-fold in the earliest passage to 1.3-fold in the latest passage group. Collectively, these in vitro experiments demonstrate that despite the consistent and stable expression of endothelial markers, cbEPCs undergo cellular and functional changes as they are expanded in culture. Their morphology, growth kinetics, and proliferative responses toward angiogenic growth factors progressively resembled those of HDMECs, indicating a process of in vitro cell maturation over time. We showed previously that proliferative responses of HDMECs isolated in our laboratory do not change from passage 3 to 12.[21]

Effect of in vitro expansion of cbEPCs on in vivo vasculogenesis

We next tested whether the maturation of cbEPCs observed during their expansion in vitro has any effect on their vasculogenic ability in vivo. To answer this question, cbEPCs at different passages (3, 6, and 12) were implanted subcutaneously into nude mice in the presence of HSVSMCs. Examination after one week of the

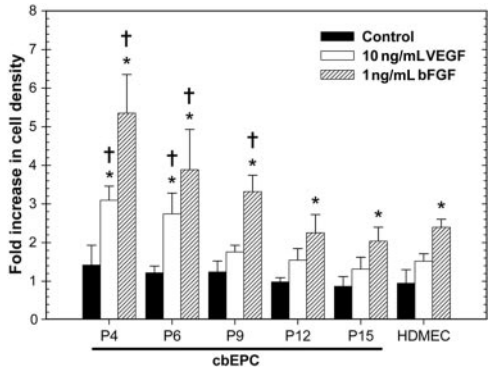

Figure 4. Proliferative response toward angiogenic factors of EPCs. cbEPCs at different passage numbers (P4, P6, P9, P12, and P15) were seeded on FN-coated plates in EMB-2 supplemented with 5% FBS (control medium). After the initial 24-hour period, cells were treated with control medium in the presence or absence of either 10 ng/mL VEGF or 1 ng/mL bFGF and assayed for cell number after 48 hours. Each bar represents the mean of 3 separate cultures ± SD, with values normalized to the values of cell density obtained at 24 hours when treatment began. *$P < .05$ compared with control. †$P < .05$ compared with equivalent treatment on HDMECs.

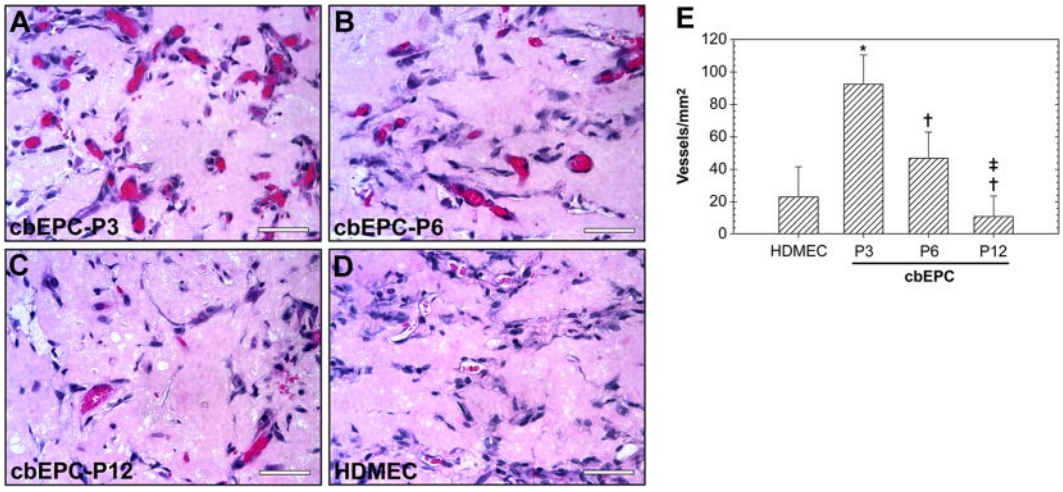

Figure 5. Effect of in vitro expansion of EPCs on in vivo vasculogenesis. Matrigel implants containing cbEPCs and HSVSMCs (4:1 ratio) were evaluated after one week. (A-C) H&E staining of Matrigel implants (× 400) containing cbEPCs at passages 3 (A), 6 (B), and 12 (C). HDMECs implants (with HSVSMCs; 4:1 ratio) were used as control for mature ECs (D; × 400). All images are representative of implants harvested from 4 different animals (scale bar represents 50 μm). (E) Microvessel density in Matrigel implants was quantified by counting lumenal structures containing red blood cells. Each bar represents the mean microvessel density value determined from 4 separated implants and animals ± SD. *$P < .05$ compared with HDMEC. †$P < .05$ compared with cbEPC-P3. ‡$P < .05$ compared with cbEPC-P6.

H&E-stained implants (Figure 5A-D) revealed a difference in the level of in vivo vascularization. Quantification of the red blood cell–containing microvessels (Figure 5E) showed that the differences among the groups were statistically significant ($P < .05$) in all the cases, with values ranging from 93 ± 18 vessels/mm^2 when using cbEPCs at passage 3 to 11 ± 13 vessels/mm^2 with passage 12. These results show that expansion of the cell population in vitro has indeed a significant impact in the subsequent performance in vivo. Parallel evaluation using mature HDMECs also revealed the presence of 23 ± 19 vessels/mm^2. This number of microvessels was inferior to those generated by the earliest passages of cbEPCs (passages 3 and 6), with values significantly higher in the case of cbEPCs at passage 3. In contrast, HUVECs combined with HSVSMCs formed 52 ± 9 vessels/mm^2 (data not shown), indicating a robust vasculogenic potential from this source of ECs.

We tested whether the lower vasculogenic ability observed in expanded cbEPCs could be compensated for by increasing the initial number of EPCs seeded into the implants. To evaluate this, we implanted either 0.5×10^6 (referred to as × 1/3), 1.5×10^6 (× 1), or 4.5×10^6 (× 3) cbEPCs at passages 6 and 12 (Figure 6) in the presence of HSVSMCs at a constant 4:1 ratio. One week after xenografting, examination of the H&E-stained implants (Figure 6A-F) revealed that an increase in the number of cbEPCs resulted in a higher degree of in vivo vascularization. Quantification of the microvessel densities (Figure 6J) showed that the differences among the groups of cbEPCs at passage 6 were statistically

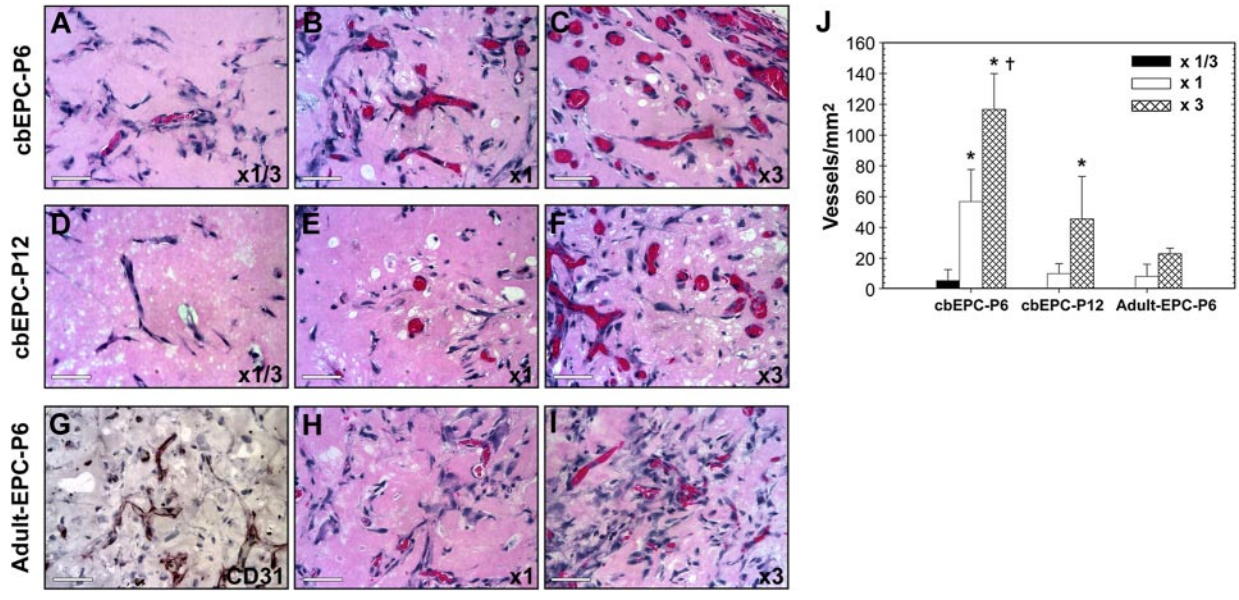

Figure 6. Effect of implanted cell number on vasculogenic performance of EPCs. Matrigel implants containing either 0.5×10^6 (× 1/3) (A,D), 1.5×10^6 (× 1) (B,E,H), or 4.5×10^6 (× 3) (C,F,I) EPCs in the presence of HSVSMCs (4:1 EPCs/HSVSMCs ratio) were evaluated after one week. (A-C) H&E staining of Matrigel implants containing cbEPCs at passage 6 (× 400); (D-F) cbEPCs at passage 12 (× 400); and (G-I) adult EPCs at passage 6 (× 400). (G) Anti–human CD31 immunostained section of adult EPCs at passage 6 seeded at × 3. All images are representative of implants harvested from 4 different animals (scale bar represents 50 μm). (J) Microvessel density was quantified by counting lumenal structures containing red blood cells. Each bar represents the mean microvessel density value determined from 4 separated implants and animals ± SD. *$P < .05$ compared with × 1/3. †$P < .05$ compared with × 1.

significant ($P < .05$), with values ranging from 6 ± 7 vessels/mm^2 to 117 ± 23 vessels/mm^2 when using $\times$ 1/3 or $\times$ 3, respectively. Consistent with the previous results (Figure 5), the values of microvessel density in implants of cbEPCs at passage 6 were always higher than those at passage 12 when the same numbers of cbEPCs were used; indeed no microvessels were detected with $\times$ 1/3 passage 12 cells. Nevertheless, at passage 12, the partial loss of vasculogenic potential was compensated by increasing the number of seeded cells. As seen in Figure 6D-F,J, by simply seeding the implants with 3 times higher density of cbEPCs at passage 12, microvessel density was raised from 10 ± 6 vessels/mm^2 ($\times$ 1) to 46 ± 28 vessels/mm^2 ($\times$ 3). Furthermore, the microvessel level achieved with $\times$ 3 passage 12 cells was similar to the level achieved with passage 6 cells at $\times$ 1 ($P = .56$).

We evaluated whether a similar approach (ie, increasing the number of EPCs seeded) would result in increased vasculogenesis when using EPCs isolated from blood of adult volunteers (Figure S5). To test this, we implanted either 1.5×10^6 ($\times$ 1) or 4.5×10^6 ($\times$ 3) adult EPCs at passage 6 in the presence of HSVSMCs (4:1 ratio). One week after xenografting, examination of the H&E-stained sections (Figure 6H-I) and human CD31-specific immunostaining (Figure 6G) revealed the presence of human microvessels containing red blood cells in both cases. As occurred with cbEPCs, we found that an increase in the number of adult EPCs resulted in a higher degree of in vivo vascularization with values ranging from 8 ± 8 lumens/mm^2 to 23 ± 4 lumens/mm^2 when using $\times$ 1 or $\times$ 3 adult EPCs, respectively. Quantification of the microvessel densities (Figure 6J) showed that adult EPCs at $\times$ 3 was similar to cbEPC-P6 $\times$ 1 ($P = .10$) and cbEPC-P12 $\times$ 3 ($P = .2$). In summary, these in vivo experiments clearly show that in addition to the cellular and functional changes observed in vitro, the vasculogenic ability of expanded EPCs progressively diminished but that this effect can be compensated for by increasing the number of EPCs initially seeded in Matrigel.

Discussion

Tissue vascularization is one of the major challenges to be addressed for the therapeutic success of TE applications. Here, we show that blood-derived EPCs have an inherent vasculogenic ability that can be exploited to create functional microvascular networks in vivo. Implantation of EPCs with HSVSMCs resulted in the formation of an extensive blood vessel network after one week. The presence of human EC-lined lumens containing murine erythrocytes throughout the implants indicated not only a process of vasculogenesis by the implanted cells, but also the formation of functional anastomoses with the host circulatory system. Our results are the first to demonstrate the in vivo vasculogenic potential of blood-derived EPCs in a TE setting. Based on our results, we speculate that microvascular networks could be formed in many types of TE constructs with use of blood-derived EPCs.

Previous investigators have suggested the possibility of creating microvascular networks using mature ECs derived from vascular tissue. Both HUVECs and HDMECs, seeded into collagen/fibronectin gels and biopolymer matrices, respectively, were shown to form complex vascular structures perfused by the host circulation after implantation into immunodeficient mice.[12,13] Alternatively, the use of fat-derived vessel fragments embedded into collagen gels was shown to generate perfused microvessels in immunodeficient mice.[30] Nevertheless, the necessity of invasive procedures together with their limited proliferative and vasculogenic ability represents important constraints for the clinical use of mature ECs derived from autologous vascular tissue.

For therapeutic applications, one critical requisite will be to isolate defined populations of cells so that growth and differentiation can be controlled and regulated during tissue development. Since first identified,[16] EPCs have been isolated from the MNC fraction of blood in numerous studies.[5,18-20,24,31,32] However, their phenotypical characterization has been often controversial.[20] In our study, we show that 10^{11} homogeneous EPCs can be obtained from 25 to 50 mL cord blood after 30 days in culture and 10^8 EPCs from 50 mL adult peripheral blood. These cell numbers are likely to exceed, in the case of cord blood, and be sufficient, in the case of adult blood, what would be needed for most TE applications. Hence, we foresee that adult blood will also be a feasible source of EPCs for autologous TE and regenerative therapies. In summary, this remarkable yield confirms peripheral blood as a robust source of ECs for autologous TE. Furthermore, our data demonstrate that these cells maintain both the expression of endothelial markers and functions through prolonged periods in culture.

As we previously demonstrated in vitro,[17] the presence of vascular smooth muscle cells in the implants was found to be critical. Seeding cbEPCs with HSVSMCs dramatically enhanced the assembly of CD31$^+$ cells into microvessel structures. Although the mechanisms by which the implanted smooth muscle cells facilitate the formation of vascular structures need to be further investigated, this finding is consistent with the extensive literature on endothelium–smooth muscle cell interactions in vascular development.[27-29] In our implants, α-SMA–positive cells were detected both around the lumenal structures and throughout the Matrigel, suggesting an ongoing process of vessel assembly, maturation, and stabilization.[27,28] We are currently investigating alternative sources that could provide autologous smooth muscle cells without the necessity of invasive procedures.

For TE applications, it is of most interest to determine the time course and the sequence of events that leads to the formation of functional microvessels. Time course analyses of the implants revealed that cells appeared dispersed throughout the implant by day 2. Thereafter, cells became organized into tubular structures without red blood cells by day 4, and formed functional erythrocyte-filled microvessels by day 7. Hence, our in vivo model of tissue vascularization is well suited for the study of the physiology of microvessel development and for the investigation of strategies to accelerate neovascularization. We speculate that, in Matrigel, these vessels would regress after some period of time due to the lack of metabolic demand. In future studies, the usefulness of this approach for tissue vascularization will be tested by incorporating EPCs into tissue or organ constructs that require a blood supply.

Another important finding of our study is related to the consequences the in vitro expansion had on vasculogenic ability. In previous work, we reported that far from remaining constant, the migratory capacity of EPCs in vitro decreased over time in culture.[33] Consistent with this concept, we have now shown that as cbEPCs were expanded in culture, their morphology, growth kinetics, and proliferative responses toward angiogenic growth factors progressively resembled those of HDMECs, indicating a process of in vitro cell maturation over time. In addition, this maturation correlated with a decrease in the degree of vascularization in vivo (Figure 5). Even though at first examination this finding may seem to impose a limitation on the extent to which cbEPCs could be expanded in vitro prior to implantation, we showed that the partial loss of vasculogenic ability can be compensated for by increasing the number of EPCs seeded into the implants (Figure 6). The number of EPCs in adult blood is known to be significantly lower than in cord blood,[34] which implies a more extensive expansion in vitro or greater

starting volume will be needed to obtain a sufficient number. In addition, adult EPCs are also known to have an inherently lower proliferative capacity in vitro,[18] which agrees with their lower vasculogenic ability in vivo reported here. Nevertheless, as occurred with cbEPCs after extensive expansion, these apparent limitations were overcome by increasing the number of adult EPCs seeded into the implants (Figure 6). Therefore, we speculate that the in vivo vasculogenic ability of EPCs from cord blood or adult peripheral blood can be modulated to the desired degree of vascularization.

In summary, our results strongly support the therapeutic potential of using human EPCs to form vascular networks that will allow sufficient vascularization of engineered organs and tissues. For infants, other sources such as HUVECs may also be isolated and used for this purpose. Further efforts are required to implement strategies for controlled vasculogenesis in tissue-engineered constructs using both autologous vascular endothelial and smooth muscle cells obtained from adult blood.

Acknowledgments

This work was supported by funding from the US Army Medical Research and Materiel Command (W81XWH-05-1-0115).

We thank Dr M. Aikawa for providing HSVSMCs (Brigham and Women's Hospital) and thank J. Wylie-Sears and T. Bartch for technical assistance.

Authorship

Contribution: J.M.M.-M. designed, executed, and interpreted all experiments and wrote the first draft of the paper; Z.A.K. performed RT-PCR analyses and provided intellectual advice and assistance with all aspects of the animal studies; A.P. contributed intellectual advice and technical assistance with mouse studies; X.W. provided invaluable expertise in the early stages of isolating cord blood cells; S.P. performed analyses of adhesion molecule expression; J.B. was involved in conceptual design of this project, interpretation of experimental results, and writing and editing drafts of the paper and figures.

Conflict-of-interest disclosure: The authors declare no competing financial interests.

Correspondence: Joyce Bischoff, Vascular Biology Research Program and Department of Surgery, Children's Hospital Boston, Harvard Medical School, Boston, MA 02115; e-mail: joyce.bischoff@childrens.harvard.edu.

References

1. Vacanti JP, Langer R. Tissue engineering: the design and fabrication of living replacement devices for surgical reconstruction and transplantation. Lancet. 1999;354(suppl 1):SI32-S134.
2. Langer R, Vacanti JP. Tissue engineering. Science. 1993;260:920-926.
3. Stock UA, Sakamoto T, Hatsuoka S, et al. Patch augmentation of the pulmonary artery with bioabsorbable polymers and autologous cell seeding. J Thorac Cardiovasc Surg. 2000;120:1158-1167; discussion 1168.
4. Hoerstrup SP, Sodian R, Daebritz S, et al. Functional living trileaflet heart valves grown in vitro. Circulation. 2000;102(19 Suppl 3):III44-III49.
5. Kaushal S, Amiel GE, Guleserian KJ, et al. Functional small-diameter neovessels created using endothelial progenitor cells expanded ex vivo. Nat Med. 2001;7:1035-1040.
6. Shieh SJ, Vacanti JP. State-of-the-art tissue engineering: from tissue engineering to organ building. Surgery. 2005;137:1-7.
7. Chrobak KM, Potter DR, Tien J. Formation of perfused, functional microvascular tubes in vitro. Microvasc Res. 2006;71:185-196.
8. Nomi M, Atala A, Coppi PD, Soker S. Principals of neovascularization for tissue engineering. Mol Aspects Med. 2002;23:463-483.
9. Lee H, Cusick RA, Browne F, et al. Local delivery of basic fibroblast growth factor increases both angiogenesis and engraftment of hepatocytes in tissue-engineered polymer devices. Transplantation. 2002;73:1589-1593.
10. Ochoa ER, Vacanti JP. An overview of the pathology and approaches to tissue engineering. Ann N Y Acad Sci. 2002;979:10-26; discussion 35-38.
11. Peters MC, Polverini PJ, Mooney DJ. Engineering vascular networks in porous polymer matrices. J Biomed Mater Res. 2002;60:668-678.
12. Schechner JS, Nath AK, Zheng L, et al. In vivo formation of complex microvessels lined by human endothelial cells in an immunodeficient mouse. Proc Natl Acad Sci U S A. 2000;97:9191-9196.
13. Nor JE, Peters MC, Christensen JB, et al. Engineering and characterization of functional human microvessels in immunodeficient mice. Lab Invest. 2001;81:453-463.
14. Rafii S, Lyden D. Therapeutic stem and progenitor cell transplantation for organ vascularization and regeneration. Nat Med. 2003;9:702-712.
15. Levenberg S, Rouwkema J, Macdonald M, et al. Engineering vascularized skeletal muscle tissue. Nat Biotechnol. 2005;23:879-884.
16. Asahara T, Murohara T, Sullivan A, et al. Isolation of putative progenitor endothelial cells for angiogenesis. Science. 1997;275:964-967.
17. Wu X, Rabkin-Aikawa E, Guleserian KJ, et al. Tissue-engineered microvessels on three-dimensional biodegradable scaffolds using human endothelial progenitor cells. Am J Physiol Heart Circ Physiol. 2004;287:H480-H487.
18. Ingram DA, Mead LE, Tanaka H, et al. Identification of a novel hierarchy of endothelial progenitor cells using human peripheral and umbilical cord blood. Blood. 2004;104:2752-2760.
19. Lin Y, Weisdorf DJ, Solovey A, Hebbel RP. Origins of circulating endothelial cells and endothelial outgrowth from blood. J Clin Invest. 2000;105:71-77.
20. Yoder MC, Mead LE, Prater D, et al. Redefining endothelial progenitor cells via clonal analysis and hematopoietic stem/progenitor cell principals. Prepublished on October 19, 2006, as DOI 10.1182/blood-2006-08-043471. (Now available as Blood. 2007;109:1801-1809.)
21. Kraling BM, Bischoff J. A simplified method for growth of human microvascular endothelial cells results in decreased senescence and continued responsiveness to cytokines and growth factors. In Vitro Cell Dev Biol Anim. 1998;34:308-315.
22. Melero-Martin JM, Dowling MA, Smith M, Al-Rubeai M. Optimal in-vitro expansion of chondroprogenitor cells in monolayer culture. Biotechnol Bioeng. 2006;93:519-533.
23. Rehman J, Li J, Orschell CM, March KL. Peripheral blood "endothelial progenitor cells" are derived from monocyte/macrophages and secrete angiogenic growth factors. Circulation. 2003;107:1164-1169.
24. Gulati R, Jevremovic D, Peterson TE, et al. Diverse origin and function of cells with endothelial phenotype obtained from adult human blood. Circ Res. 2003;93:1023-1025.
25. Parums DV, Cordell JL, Micklem K, Heryet AR, Gatter KC, Mason DY. JC70: a new monoclonal antibody that detects vascular endothelium associated antigen on routinely processed tissue sections. J Clin Pathol. 1990;43:752-757.
26. Levenberg S, Huang NF, Lavik E, Rogers AB, Itskovitz-Eldor J, Langer R. Differentiation of human embryonic stem cells on three-dimensional polymer scaffolds. Proc Natl Acad Sci U S A. 2003;100:12741-12746.
27. Folkman J, D'Amore PA. Blood vessel formation: what is its molecular basis? Cell. 1996;87:1153-1155.
28. Darland DC, D'Amore PA. Blood vessel maturation: vascular development comes of age. J Clin Invest. 1999;103:157-158.
29. Darland DC, D'Amore PA. Cell-cell interactions in vascular development. Curr Top Dev Biol. 2001;52:107-149.
30. Shepherd BR, Chen HY, Smith CM, Gruionu G, Williams SK, Hoying JB. Rapid perfusion and network remodeling in a microvascular construct after implantation. Arterioscler Thromb Vasc Biol. 2004;24:898-904.
31. Shi Q, Rafii S, Wu MH, et al. Evidence for circulating bone marrow-derived endothelial cells. Blood. 1998;92:362-367.
32. Hristov M, Erl W, Weber PC. Endothelial progenitor cells: isolation and characterization. Trends Cardiovasc Med. 2003;13:201-206.
33. Khan ZA, Melero-Martin JM, Wu X, et al. Endothelial progenitor cells from infantile hemangioma and umbilical cord blood display unique cellular responses to endostatin. Blood. 2006;108:915-921.
34. Peichev M, Naiyer AJ, Pereira D, et al. Expression of VEGFR-2 and AC133 by circulating human CD34(+) cells identifies a population of functional endothelial precursors. Blood. 2000;95:952-958.

Supplemental File

Methods for Phenotypic Characterization of EPCs

Flow cytometry

Cytometric analyses of cells were carried out by labeling with fluorescein isothiocyanate (FITC)-conjugated mouse anti-human CD31 (Ancell, Bayport, MN), FITC-mouse anti-human CD146 (Chemicon International), phycoerythrin (PE)-conjugated mouse anti-human CD34, PE-mouse anti-human Neuropilin-1 (Miltenyi Biotec, Auburn, CA), PE-mouse anti-human VEGF-R2 (R&D Systems, Minneapolis, MN), FITC-mouse anti-human CD45, FITC-mouse anti-human CD14, FITC-mouse-IgG_1, PE-mouse IgG_1 (BD PharMingen, San Jose, CA), PE-mouse anti-human CD90 (Chemicon International), PE-mouse anti-human CD105 (Serotec, Raleigh, NC) antibodies. Additionally, 4% paraformaldehyde-fixed, 0.5% saponin-permeabilized cells were incubated with mouse anti-human von Willebrand factor (vWF; DakoCytomation, Carpinteria, CA), and rabbit anti-human Flt-1 (Santa Cruz Biotecnology, Santa Cruz, CA) antibodies followed by FITC-conjugated secondary antibody (Vector Laboratories, Burlingame, CA). Antibody labeling was carried out for 20 minutes on ice followed by 3 washes with PBS/1% BSA/0.2 mM ethylenediaminetetraacetic acid (EDTA) and resuspension in 1% paraformaldehyde. Flow cytometric analyses were performed using a Becton Dickinson FACScan flow cytometer.

Indirect immunofluorescence

Immunofluorescence was carried out using goat anti-human CD31 (Santa Cruz Biotecnology), mouse anti-human VE-cadherin (Immunotech, Westbrook, ME), mouse anti-human vWF (DakoCytomation), mouse anti-human α-smooth muscle actin (α-SMA; Sigma-Aldrich) and mouse anti-human Calponin (DakoCytomation) antibodies, followed by FITC-conjugated secondary antibodies (Vector Laboratories) and VECTASHIELD mounting medium with 4,6diamidino-2-phenylindole (DAPI) (Vector Laboratories). Images were taken with a Nikon

Eclipse TE300 (Nikon, Melville, NY) using Spot Advance 3.5.9 software (Diagnostic Instruments, Sterling Heights, MI) and 20x/0.45 objective lens.

RT-PCR

cDNA synthesis from total RNA was performed with primers for human CD31, CD34, CD105, VEGF-R2, VE-cadherin, vWF, eNOS and ribosomal S9 [1,2]. The reactions were performed for 35 cycles as follows: 95^{o}C for 3 minutes (initiation; 30 seconds/cycle thereafter), 55^{o}C for 30 seconds, and 72^{o}C for 45 seconds.

Adhesion molecules assay

Leukocyte adhesion molecules were analyzed after treatment with or without 10 ng/ml of tumor necrosis factor-α (TNF-α; R&D Systems) for 5 hours [3] by labeling with mouse anti-human E-selectin, mouse anti-human ICAM-1 or mouse anti-human VCAM-1 followed by secondary FITC-conjugated anti-mouse IgG. Mouse IgG1 (DakoCytomation) was used as isotype-control.

Western blotting

Cells were lysed with 4 mol/L urea, 0.5% SDS, 0.5% NP-40, 100 mmol/L Tris, and 5 mmol/L EDTA, pH 7.4, containing 100 μmol/L leupeptin, 10 mmol/L benzamidine, 1 mmol/L PMSF, and 12.5 μg/ml aprotinin. Lysates were subjected to 10% SDS-PAGE (10 μg of protein per lane) and transferred to Immobilon-P membrane. Membranes were incubated with respective primary Abs, goat anti-human CD31, goat anti-human PDGF-Rβ (Santa Cruz Biotecnology), and mouse anti-human Tubulin (Sigma-Aldrich) diluted in 1x PBS, 5% dry milk, 0.1% Tween-20, and then with secondary Ab (peroxidase-conjugated anti-goat or anti-mouse). Antigen-Ab complexes were visualized using Lumiglo and chemiluminescent sensitive film.

References

1. Murga M, Yao L, Tosato G. Derivation of endothelial cells from CD34- umbilical cord blood. Stem Cells. 2004;22:385-395.
2. Khan ZA, Melero-Martin JM, Wu X, et al. Endothelial progenitor cells from infantile hemangioma and umbilical cord blood display unique cellular responses to endostatin. Blood. 2006;108:915-921.
3. Dvorin EL, Jacobson J, Roth SJ, Bischoff J. Human pulmonary valve endothelial cells express functional adhesion molecules for leukocytes. J Heart Valve Dis. 2003;12:617-624.

Supplemental Figure 1

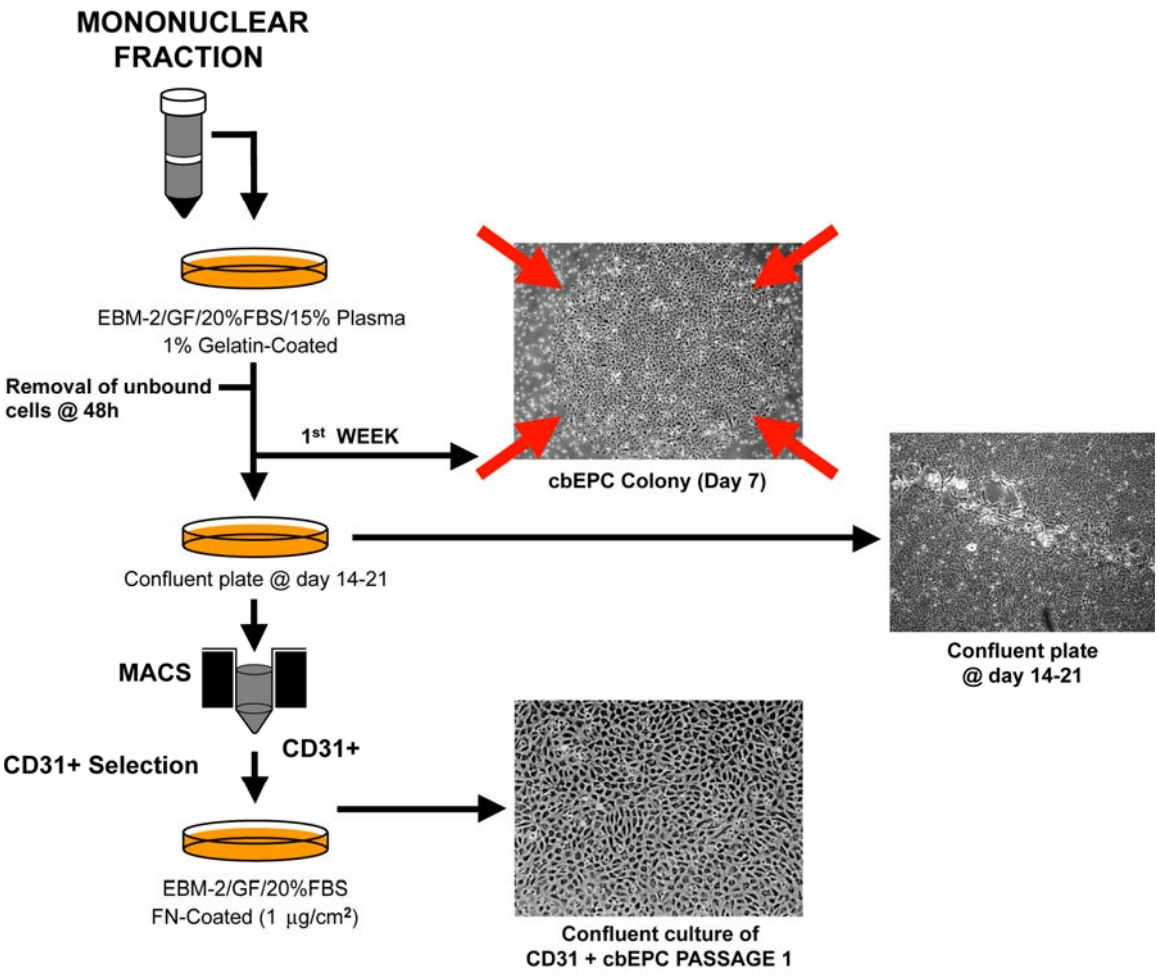

Figure S1. Isolation of cord blood EPCs. Cord blood-derived EPCs (cbEPCs) were obtained from the mononuclear cell (MNC) fractions of 25 mL umbilical cord blood samples. MNCs were seeded on 1% gelatin-coated tissue culture plates using EBM-2 supplemented with SingleQuots, 20% FBS, 1x glutamine-penicillin-streptomycin (GPS) and 15% autologous plasma. Unbound cells were removed at 48 hours and the bound fraction was maintained in culture using EBM-2 supplemented with 20% FBS, SingleQuots and 1x GPS (EBM-2/20%). Colonies of endothelial-like cells were allowed to grow until confluent, trypsinized and purified using CD31-coated magnetic beads. CD31-selected cbEPCs were serially passaged and cultured on fibronectin-coated (FN; 1 ug/cm^2) plates at 5x10^3 cell/cm^2 in EBM-2/20%.

Supplemental Figure 2

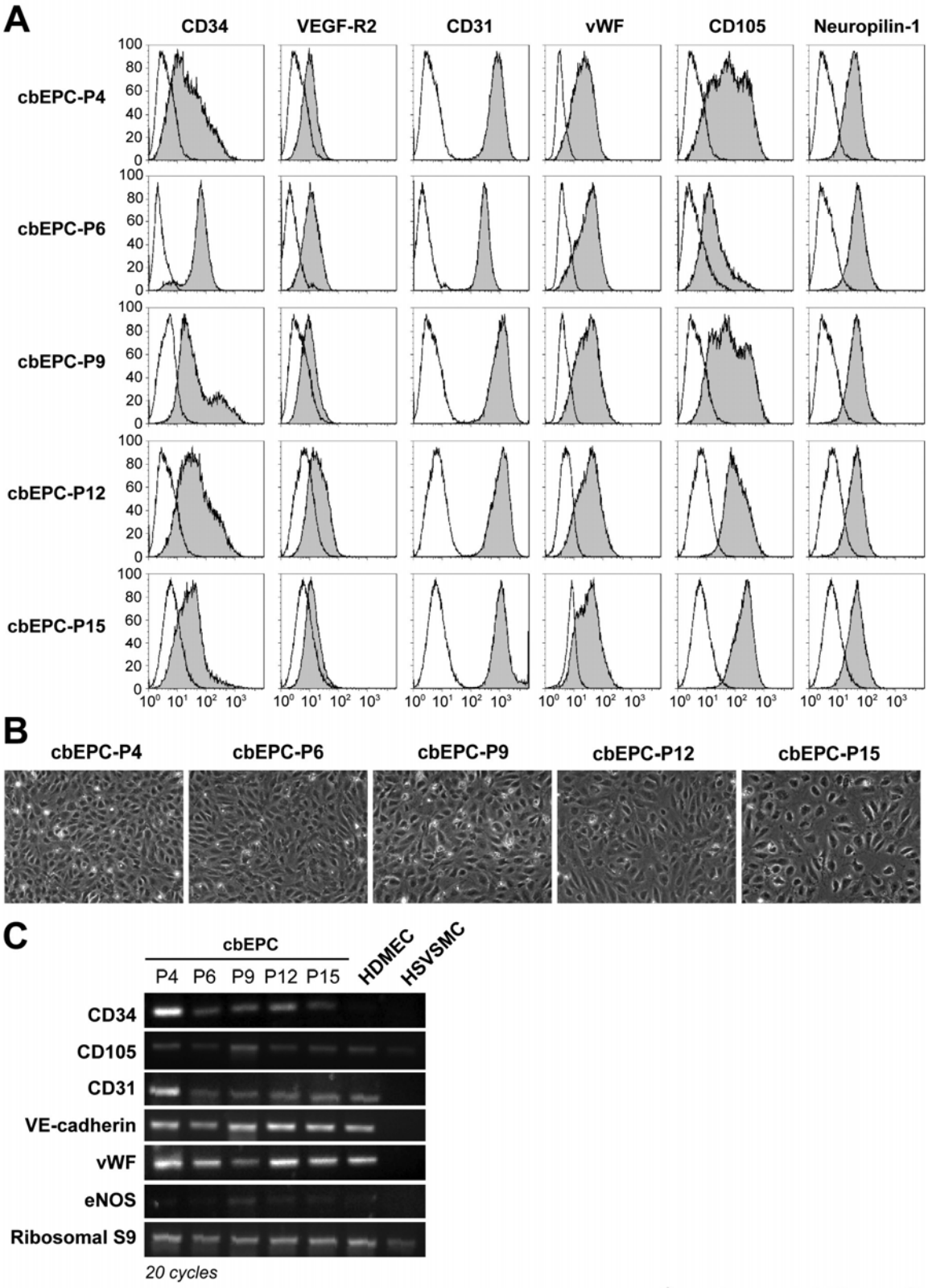

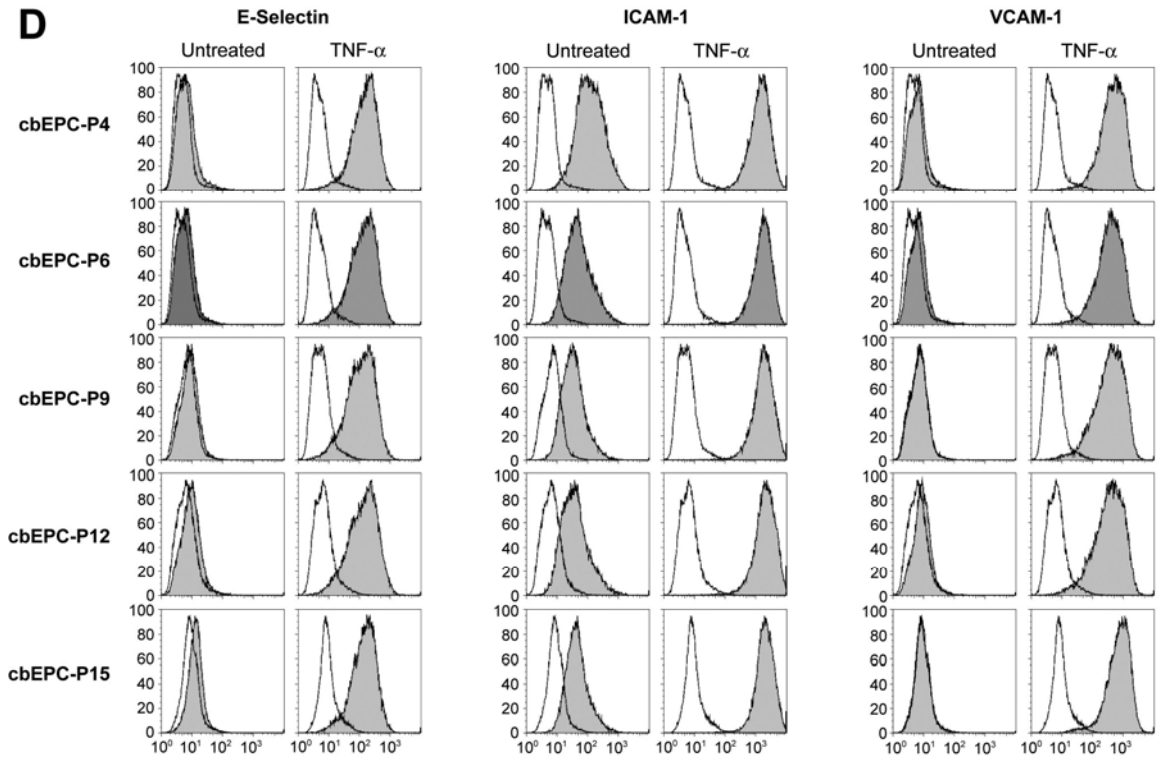

Figure S2. Phenotypic characterization of cbEPCs at different passages. CD31-selected cbEPCs were evaluated at passages 4, 6, 9, 12 and 15. HDMECs and HSVSMCs served as positive and negative controls respectively. (A) Cytometric analysis of cultured cbEPCs for endothelial markers CD34, VEGF-R2, CD31, vWF, CD105 and Neuropilin-1. Solid gray histograms represent cells stained with fluorescent antibodies. Isotype-matched controls are overlaid in a black line on each histogram. (B) Phase microscopy pictures of cultured cbEPCs grown in confluent monolayer and showing characteristic cobblestone morphology. (C) RT-PCR analysis of cbEPCs for endothelial markers CD34, CD105, CD31, VE-cadherin, vWF and eNOS. (D) Up-regulation of E-selectin, ICAM-1 and VCAM-1 in cultured cbEPC in response to TNF-α. Solid gray histograms represent cells stained with fluorescent antibodies while black lines correspond to the isotype-matched control fluorescent antibodies.

Supplemental Figure S3

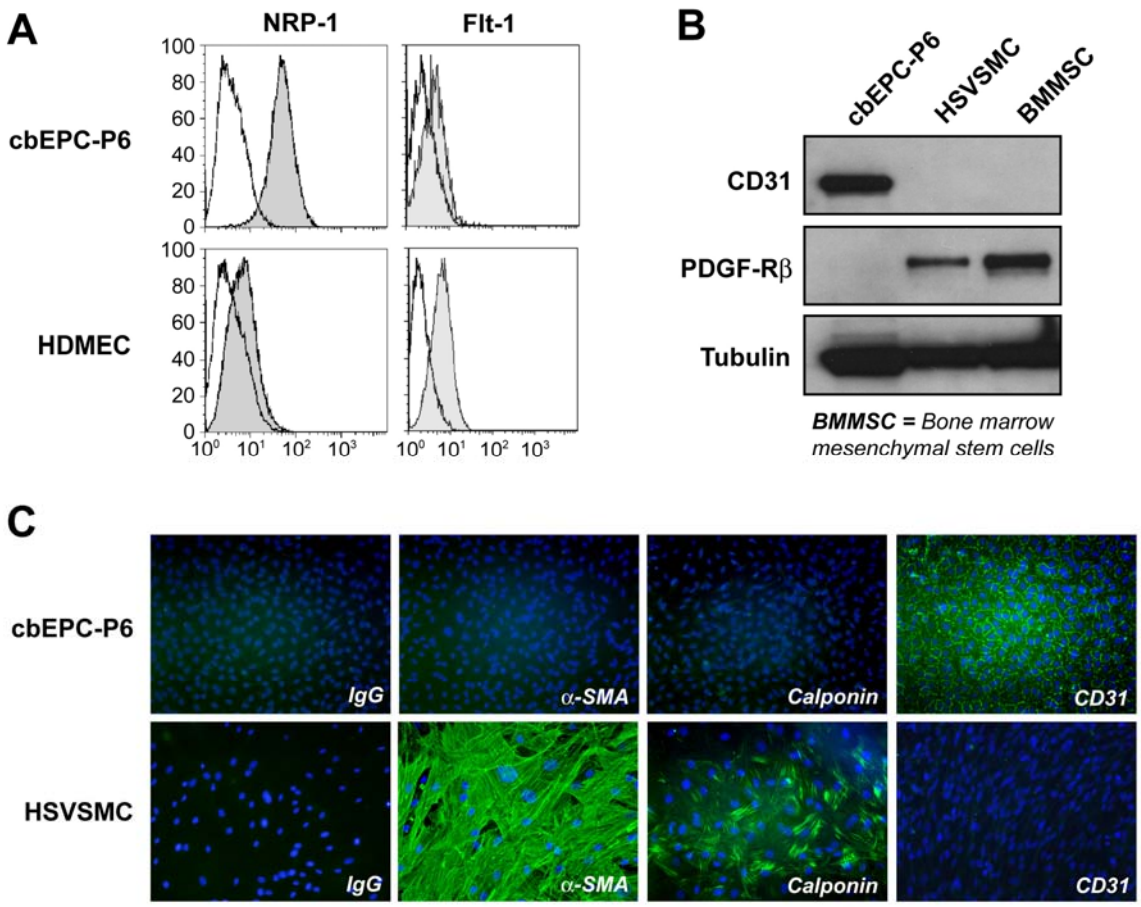

Figure S3. Further phenotypic characterization of cbEPCs. CD31-selected cbEPCs were evaluated at passages 6. HDMECs served as positive control while HSVSMCs and BMMSCs served as negative controls. (A) Cytometric analysis of cultured cbEPCs for VEGF-receptors neuropilin-1 (NRP-1) and Flt-1 (VEGF-R1). Solid gray histograms represent cells stained with fluorescent antibodies. Isotype-matched controls are overlaid in a black line on each histogram. (B) Western blotting of cultured cbEPCs showing positive reaction for CD31 and negative reaction for smooth mucle/mesenchymal cell receptor PDGF-Rβ. (C) Indirect immunofluorescence of cultured cbEPCs grown in confluent monolayer showing positive staining for CD31 and negative staining for smooth muscle/mesenchymal cell markers α-SMA and calponin.

Supplemental Figure 4

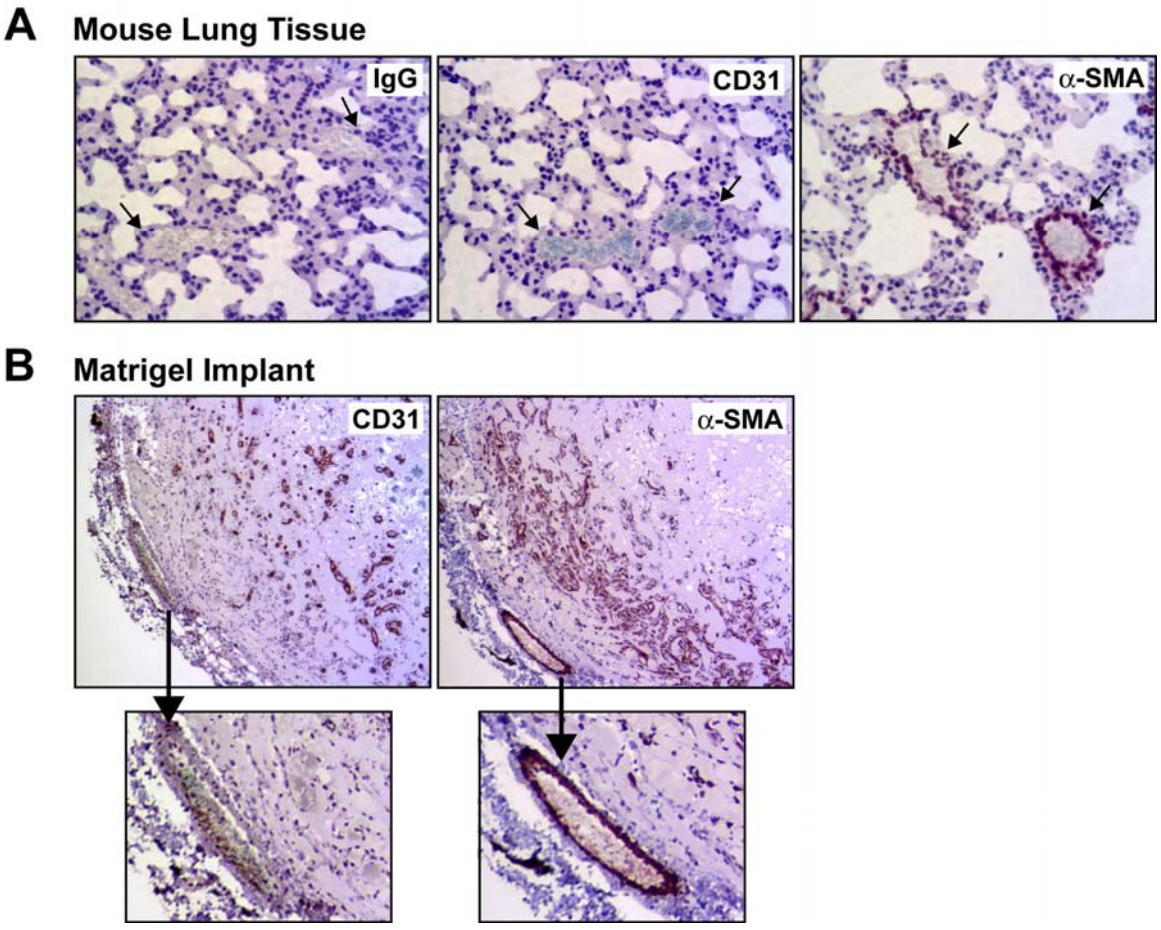

Figure S4. Species specificity of anti-human CD31 and anti-α-SMA antibodies. (A) The specificity of the anti-human CD31 antibody was confirmed by the negative reaction obtained when mouse lung tissue sections were stained. The α-SMA antibody was not human-specific, as shown by the positive staining of mouse lung tissue sections. (B) Immunohistochemical staining of the Matrigel implants (prepared as described in Figure 2 of the manuscript) using human specific CD31 antibody and α-SMA antibody reveals the presence of human lumenal structures throughout the xenografts. Higher magnifications of a mouse vessel adjacent to the implant shows negative reaction for CD31, confirming the specificity of the human CD31 antibody. All images are representative of implants harvested from four different animals.

Supplemental Figure 5

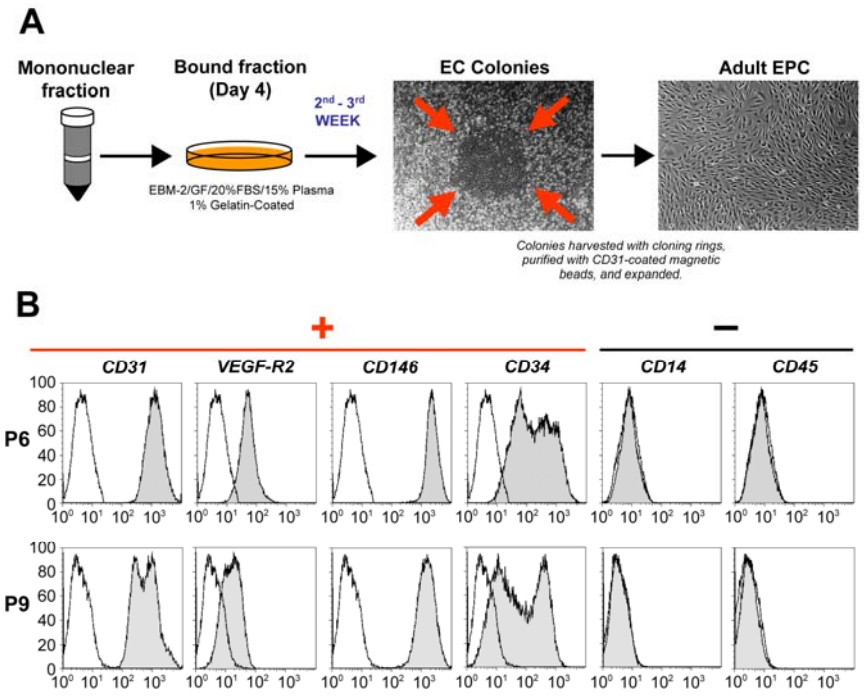

Figure S5. Isolation of adult peripheral blood EPCs. (A) Adult peripheral blood-derived EPCs (adult EPCs) were obtained from the mononuclear cell (MNC) fractions of 50 mL peripheral blood samples from healthy volunteer donors. MNCs were seeded on 1% gelatin-coated tissue culture plates using EBM-2 supplemented with SingleQuots, 20% FBS, 1x GPS and 15% autologous plasma. Unbound cells were removed at 4 days and the bound fraction was maintained in culture using EBM-2 supplemented with 20% FBS, SingleQuots and 1x GPS (EBM-2/20%). Colonies of endothelial-like cells were harvested using cloning rings, expanded and purified using CD31-coated magnetic beads. CD31-selected adult EPCs were serially passaged and cultured on fibronectin-coated (FN; 1 ug/cm^2) plates in EBM-2/20%. (B) Cytometric analysis of cultured adult EPCs for endothelial markers CD31, VEGF-R2, CD146 and CD34, and hematopoietic/monocytic markers CD14 and CD45 at passages 6 (P6) and 9 (P9). Solid gray histograms represent cells stained with fluorescent antibodies. Isotype-matched controls are overlaid in a black line on each histogram.